Characterising Focused Ultrasound via High Speed Shadowgraphic Imaging at 10 Million Frames Per Second

Kristoffer Johansen, Jae Hee Song, and Paul Prentice
CavLab, Cluster of Ultrasound Science, Technology and Engineering Research
University of Glasgow, UK
Email: Paul.Prentice@glasgow.ac.uk

***Abstract*—In this paper, ultra-high speed shadowgraphic imaging at 10×10^6 frames-per-second with an effective temporal resolution of 10ns per frame, is used to characterise aspects of the acoustic field, the medium of propagation, and phase characterization of a needle hydrophone. Specifically, at the third harmonic of the driving transducer, constructive and destructive interference is observed in close proximity to the needle hydrophone, due to reflections of the propagating field from the needle hydrophone. At the fundamental, speed of sound estimation from cross–correlating temporal changes in gray scale value of two individual pixels along propagating axis. Furthermore, phase characterisation of needle hydrophone from 0.7MHz to 1MHz and at 1.2MHz, using deconvolved needle hydrophone data at the fundamental driving frequency, 1.1MHz, to estimate a propagation time delay between pixel sample position and deconvolved waveform. Most reliable results for both speed of sound estimation and phase characterisation of the needle hydrophone are achieved using optical data close to the acoustic focus, where both measurements are in agreement with theory and calibration data.**

I. Introduction

Intuitively, the introduction of a hydrophone, or any other in-situ measurement device such as a thermocouple, to an acoustic field for calibration or characterization purposes, will also act to perturb the field itself [1]. It is, however, difficult to make any direct assessment of the perturbations that may occur, and therefore anticipate how they may affect any given experiment. Here, we employ ultra-high speed shadowgraphic imaging at 10 million frames per second (Mfps), to directly observe the interaction of a focused ultrasound field and the sensing tip of a typical needle hydrophone (NH) device. This technique has only recently become commercially available, where a 10ns synchronized laser pulse is used for imaging illumination. The short duration of the illumination pulse enables the imaging system to capture changes in the refractive index, as a result of the propagating acoustic field [2], [3]. Each imaging sequence is 256 frames, which allows for extended observations of how the field evolves over time. Current literature has already suggested that imaging systems which possess a shadowgraphic capability can be used for acoustic field characterisation [4]. However, in this paper, we show how unprecedented ultra-high speed shadowgraphic imaging has a greater application range then previously demonstrated.

II. Methods

The experimental arrangement depicted in Fig. 1 is used to study hydrophone–acoustic field interaction in detail, both optically and acoustically. HIFU is generated via a single element piezoceramic transducer (H-198, Sonic Concepts, USA), connected to a power amplifier (2100L, Electronic and Innovation, USA) and a waveform generator (DG4102, Rigol Technologies, China). The transducer has an outer diameter of 90 mm and is geometrically focused to 77 mm from the front face. The HIFU transducer has a natural fundamental resonance frequency at 1.1 MHz, and the 3rd harmonic at 3.3 MHz, through impedance matching networks. The NH (1.0 mm diameter, PVdF, Precision Acoustics, UK) is mounted on an xyz–manipulator (Velmex Motor, Bloomfield, NY, USA). The NH is calibrated for both magnitude and phase over a bandwidth of 125 kHz - 20 MHz in 25 kHz increments, (National Physical Laboratory (NPL), 2016),

For acoustic field interaction at the third harmonic, it is placed closer to the acoustic focus, Fig. 2 (a) and (b), and for phase characterisation of the NH and speed of sound (SOS) estimation in the propagation medium, the NH is placed vertically above the acoustic focus, Fig. 1 and Fig. 3 (a). The NH is connected to an oscilloscope (MS07104A, Agilent Technologies, USA), and data collected at 4 GSs^{-1}. The experimental configuration is contained within a custom-built chamber, measuring $420 \times 438 \times 220$ mm^3 and filled with degassed, deionized water. Two of the walls of the chamber are recessed, to allow the placement of imaging optics, facilitating a spatial resolution of $\sim 25\,\mu$m/pixel and $\sim 29\,\mu$m/pixel, for the two respective lens configurations. High-speed shadowgraphic imaging of the propagating acoustic field is undertaken, at the fundamental through a makro-lens (Zeiss 100mm f2 Makro-Planar Milvus ZF.2 Lens, Germany), and at the third harmonic through a Monozoom 7 lens system (Bausch & Lomb, USA), at 10×10^6 frames per second (HPV-X2, Shimadzu, Japan), with synchronous 10 ns laser pulses (CAVILUX Smart, Cavitar, Finland) providing the illumination and effective temporal resolution, per frame. A delay generator (DG535, Stanford Research Systems, USA) provides electronic triggering to synchronize each of the instruments.

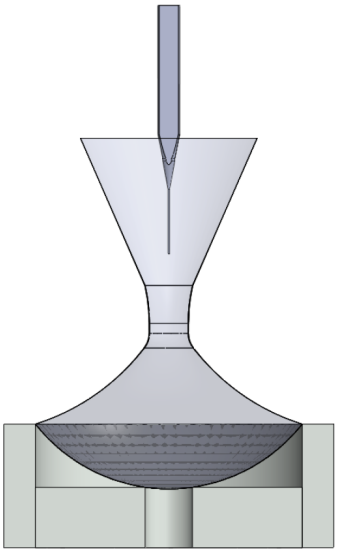

Fig. 1. Cross-section of experimental setup, illustrating the positioning of the needle hydrophone above the acoustic focus

III. Needle hydrophone–acoustic field interaction

Figure 2 shows optical and acoustic measurements of a 3.4 MHz ultrasound field. In Fig. 2 (a) and (b), changes in the refractive index of the medium, and consequently the gray scale in the images, are a manifestation of the propagating acoustic field. Both constructive and destructive interference was observed in the coloured rectangles, respectively. This is further demonstrated by Fig. 2 (c), where the variation in gray scale value, along the z-axis centred at the NH, shows the effect of interference from reflections of the NH. Examining the acoustic measurement from the NH in Fig. 2 (c) (stapled blue), it is not possible to discern how the needle is perturbing the free–field conditions. As the shadowgraphic imaging quality is highest in the acoustic focal region, these results suggest that if optical measurements of the field are to be correlated to the acoustic measurements, the NH needs to be moved further away from the acoustic focal region. In addition, the images also clearly demonstrate how diffraction correction or spatial averaging is required, as the wave-fronts incident to the NH are not plane waves, Fig 2 (a). Both of the two last remarks have been taken into account when attempting phase characterisation of the NH at the fundamental frequency of the driving transducer.

In Fig. 3 (a) high–speed shadowgraphic imaging and acoustic measurement of a 1.1 MHz ultrasound field is seen. The position of the NH is further away from the acoustic focus, relative to Fig. 2 (a,b), ensuring less interference from reflections from the NH, and planer wave-fronts being incident to the NH. These are both critical aspects of the experimental setup when correlating optical and acoustic measurements. Along the solid red line, centred at the NH, going through the acoustic focus, optical measurements of the acoustic field are undertaken. From these measurements, both phase characterisation of the

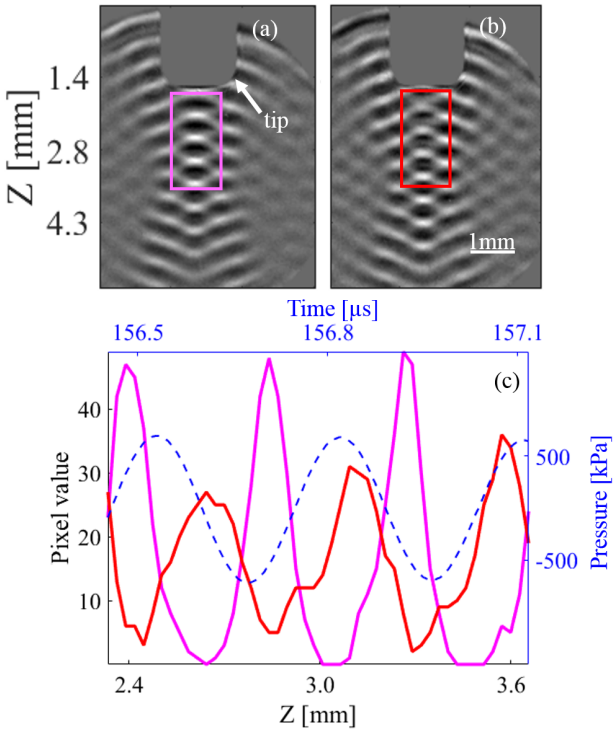

Fig. 2. Optical and acoustic measurement of 3.4 MHz ultrasound field. In (a) and (b), shadowgraphic imaging of ultrasound field, where the two frames are separated by 100 ns. Rectangular boxes (magenta and red) indicate the region of interest for constructive and deconstructive interference. In (c), needle hydrophone measurement (blue), and pixel values obtained along line centered at needle hydrophone for (a) and (b), respectively (magenta) and (red).

NH, and SOS measurements in the liquid are achieved, section IV and V. The green asterisks indicate the region where the best results are obtained, Fig 4-6.

IV. Speed of sound estimation

Speed of sound is traditionally measured using a pulse/receive system, *i.e.*, two coaxially aligned identical traducers [5]. In this paper we demonstrate that it is feasible to estimate the SOS in the propagation medium using the high speed images. The technique presented extends to both nonlinear waves and shock waves. Sampling pixels along the solid red line in Fig. 3 (a), SOS in the liquid was estimated by cross–correlation, finding the propagation time between pixels, using the following definition:

$$(g \star p)(\tau) = \int_{-\infty}^{\infty} g^*(t)p(t+\tau)dt \qquad (1)$$

where g and p represents waveforms at the two different pixel positions, g^* is the complex conjugate, and τ is the propagation time delay between two pixels. It was observed that more reasonable results were obtained when the two pixels were displaced by half a wave length, $\lambda/2$. Figure 4 shows in

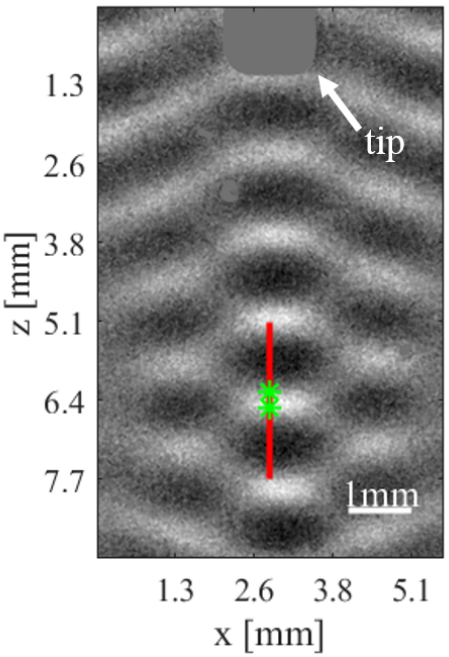

Fig. 3. In (a), high–speed shadowgraphic imaging of a 1.1 MHz ultrasound field at 10×10^6 FPS, and acoustic measurement with needle hydrophone. Red line indicates pixels are sampled for speed of sound estimation and phase characterisation of needle hydrophone.

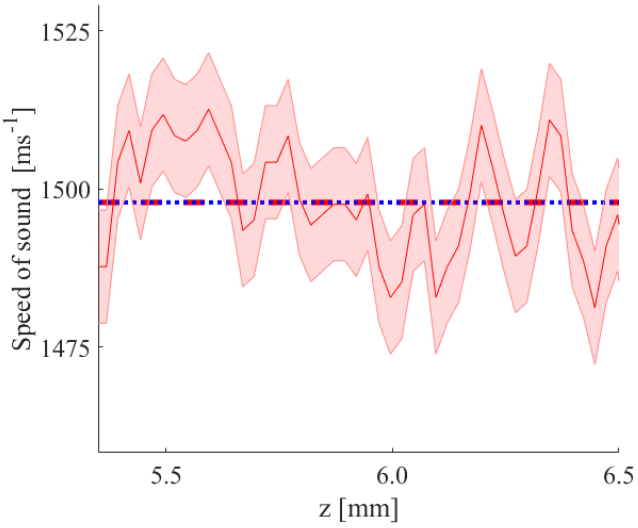

Fig. 4. In red (solid) speed of sound estimate along the red line in Fig. 2 (a) from cross correlation of pixels that are separated by $\lambda/2$, where stapled red line is the average estimated speed of sound, and dotted blue is the theoretical prediction. The shaded region represent the standard deviation of the measurement.

solid red the estimated SOS along the red line in Fig. 3 (a) using this technique, where the shading represent the standard deviation. The average estimated SOS is $1496 \pm 9\,\mathrm{ms}^{-1}$, and the theoretical prediction at 25 c° is $1497\,\mathrm{ms}^{-1}$ [6]. However, the authors would like to remark that this technique is highly sensitive to spatial calibration.

V. Phase Characterisation of Needle Hydrophone

The phase response of a NH will cause lead or lag of the incident pressure wave. This is of importance when measuring high precision transit times in fiscal measurements [7], and when deconvolving highly nonlinear pressure waves, *i.e.*, shock waves in the time domain [8], [9]. Calibrating the phase response of a hydrophone has only recently become available [10], as it is difficult to perform with adequate precision. Typical techniques include substitution calibration with a reference hydrophone, or primary calibration using optical interferometry and secondary calibration using time–delay spectrometry [11]. In this paper we show how the optical measurement of the acoustic field allows to perform phase characterisation of the NH. Assuming a linear propagating wave is observed both in the high speed images as a temporal variation of the gray scale, at a pixel along the red line in Fig. 3 (a), and at the NH. The optically measured wave has a phase delay equal to $\phi_{\mathrm{tot}} = \phi_{\mathrm{NH}} + \phi_{\mathrm{prop}}$ in the convolved NH data. Where ϕ_{NH} is equal to the phase of the NH and ϕ_{prop} is the phase due to propagation. The optically measured wave can be represented as:

$$p = P_{\mathrm{a}} \sin(\omega t + kz + \phi_{tot}) \quad , \tag{2}$$

where P_{a} is the normalised amplitude, ω is the angular frequency $2\pi f_{\mathrm{c}}$, f_{c} is the centre frequency, k is the wave-number ω/c, c is the speed of sound, and z is the position along the propagating axis. Applying full-waveform deconvolution to the NH measurement [10], with knowledge of both the magnitude and the phase, ϕ_{tot} becomes equal to ϕ_{prop}. As $\phi_{\mathrm{prop}} = \omega\tau$ where τ is the propagation time delay due to propagation from optical detection at pixel sample position to acoustic detection at the NH. The propagation time delay τ is estimated by a two step process, first the optically detected wave (stapled green) is temporally transformed, with a coarse time delay τ_1 estimated from the distance at pixel sample position to the base of the NH, assuming $c = 1497\,\mathrm{ms}^{-1}$. Secondly, the temporally transformed wave is cross–correlated with the full–waveform deconvolved NH measurement to find the fine delay τ_2, following Eq. (1).

When temporally transforming the optical measurement (stapled green), Fig. 5 (a), at pixel sample position by the propagation time delay τ, a wave which is in phase (dotted red) with the full-waveform deconvolved hydrophone (solid black) is realised, Fig. 5 (a). Assuming the propagation time delay is constant for moderate changes in frequency, a delay equal to that found at the fundamental frequency can be applied to an optically measured wave at a different frequency, and cross–correlated with the convolved NH data, Fig 5(b). The time delay between these two respective measurements is equal to the phase response of the NH ϕ_{NH} at the frequency of interest. Phase characterisation is attempted from 0.7 MHz to 1 MHz

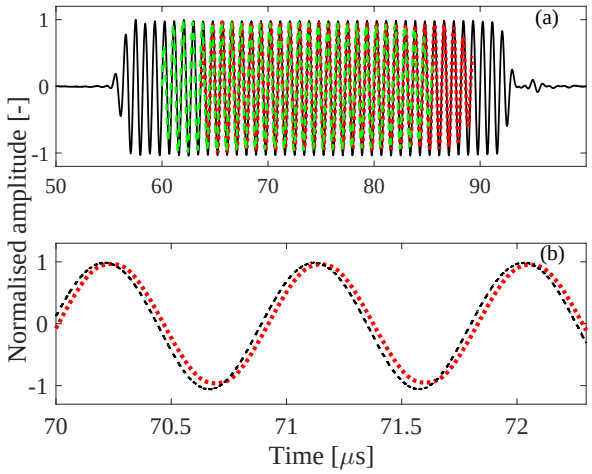

Fig. 5. Acoustical and optical measurement of ultrasonic field at 1.1 MHz. In (a), deconvolved needle hydrophone measurement (solid black), pixel sampled at midpoint (stapled green) of red line in Fig. 2 (a), and propagation time delayed pixel data (dotted red) relative to deconvolved needle. In (b), propagation time delayed (dotted red), and convolved needle hydrophone measurement (stapled black). All amplitudes are normalised to their respective maxima.

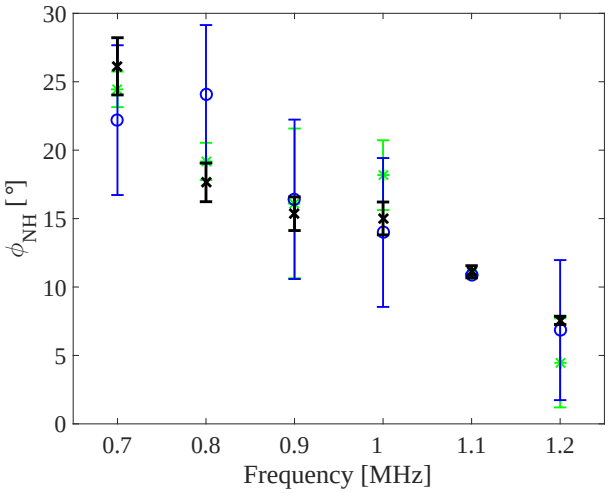

Fig. 6. Phase characterization of needle hydrophone along red line in Fig. 2 (a) using high–speed shadowgraphic imaging, where black cross is NPL calibrated phase with uncertainties, blue circle is averaged estimated phase, and green asterisks is average estimated phase in acoustic focus, Fig 3 (a). Uncertainties are represented by the standard deviation of estimated phase for respective regions.

and 1.2 MHz, using the propagation time delay estimated at 1.1 MHz. In Fig. 6 the results of phase characterisation of the NH is shown. The black-cross scatter is the NPL calibration with its respective uncertainties, blue-circle is the average phase estimated for all pixel sample positions along the red line in Fig. 3 (a), and green-asterisks is a subsection of phase characterisation data, sampled in the acoustic focus, with lower standard deviation. For all frequencies the optically estimated phase is within the uncertainty of the NPL calibration, however, large variations in estimated phase are observed as depicted by respective error bars, particularly for the whole dataset. Sampling pixels close to the acoustic focus, where the shadowgraphic imaging is of highest quality gives estimates with significantly lower standard deviation, Fig. 6.

VI. Conclusion

In conclusion we have shown that ultra-high speed shadowgraphic imaging can be used to characterise the acoustic field pattern, estimating the speed of sound in the propagation medium, and phase characterisation of a NH. Most reasonable results for speed of sound and phase characterisation of the NH are obtained in the acoustic focus, where both measurements are in agreement with theory and NPL calibration, respectively.

Acknowledgment

The research leading to these results has received funding from the European Research Council under the European Unions Seventh Framework Programme (FP/2007 2013)/ERC Grant Agreement no. 336189 (TheraCav). The authors acknowledge Keith Johnston, Graeme Casey and Miriam Jiménez García for technical assistance.

References

[1] D. R. Bacon, "Characteristics of a pvdf Membrane Hydrophone for Use in the Range 1-100 MHz," *IEEE Trans. Sonics Ultrason.*, vol. 29, no. 1, pp. 18–25, 1982.

[2] I. Thormählen, J. Straub, and U. Grigull, "Refractive Index of Water and Its Dependence on Wavelength, Temperature, and Density," *J. Phys. Chem. Ref. Data*, vol. 14, no. 4, pp. 933–945, 1985.

[3] K. Johnston, C. Tapia-Siles, B. Gerold, M. Postema, S. Cochran, A. Cuschieri, and P. Prentice, "Periodic shock-emission from acoustically driven cavitation clouds: a source of the subharmonic signal." *Ultrasonics*, vol. 54, no. 8, pp. 2151–2158, 2014.

[4] N. Kudo, "A Simple Technique for Visualizing Ultrasound Fields Without Schlieren Optics," *Ultrasound Med. Biol.*, vol. 41, no. 7, pp. 2071–2081, 2015.

[5] K. A. Wear, "The effects of frequency-dependent attenuation and dispersion on sound speed measurements: applications in human trabecular bone," *IEEE Trans. Ultrason. Ferroelectr. Freq. Control*, vol. 47, no. 1, pp. 265–273, 2000.

[6] H. Medwin, "Speed of sound in water: A simple equation for realistic parameters," *J. Acoust. Soc. Am.*, vol. 58, no. 6, pp. 1318–1319, 1975.

[7] K. K. Andersen, P. Lunde, and J. Kocbach, "Magnitude and phase reciprocity calibration of ultrasonic piezoelectric disk in air," in *Proc. 39th Scand. Symp. Phys. Acoust.*, 2016, pp. 1–21.

[8] J. H. Song, K. Johansen, and P. Prentice, "An analysis of the acoustic cavitation noise spectrum: The role of periodic shock waves," *unpublished*.

[9] K. Johansen, J. H. Song, and P. Prentice, "Deconvolution of acoustically detected bubble-collapse shock waves," *Ultrasonics, in press*.

[10] A. Hurrell, "Voltage to pressure conversion: are you getting 'phased' by the problem?" *J. Phys. Conf. Ser.*, vol. 1, pp. 57–62, 2004.

[11] V. Wilkens and C. Koch, "Amplitude and phase calibration of hydrophones up to 70 MHz using broadband pulse excitation and an optical reference hydrophone," *J. Acoust. Soc. Am.*, vol. 115, no. 6, pp. 2892 – 2903, 2004.